Nerve Fibre Extraction in Confocal Corneal Microscopy Images for Human Diabetic Neuropathy Detection using Gabor Filters

M. A. Dabbah[a,*], J. Graham[a], Mitra Tavakoli[b], Ioannis Petropoulos[b] and Rayaz A. Malik[b]

[a]ISBE , University of Manchester, Oxford Rd., M13 9PT, UK
[b]Division of Cardiovascular Medicine, University of Manchester, Oxford Rd., M13 9PT, UK

Abstract. Recently CCM images have shown a great potential to be a non-invasive and hence reiterative surrogate for accurate and reliable detection and quantification of human diabetic neuropathy. This paper presents a comparison between two methods to detect the nerves fibres in the CCM images: a well documented line operator (Linop) and a method based on Gabor filtering. The evaluation of the extraction is measured according to ground truth data that has been manually extracted. The Gabor filtering method has achieved a reduction of 11.82% in the overall EER of the Linop method at the best operation points.

1 Introduction

The accurate detection and quantification of human Diabetic Peripheral Neuropathy (DPN) are important to define at risk patients, anticipate deterioration, and assess new therapies. Current methods lack sensitivity, require expert assessment and focus only on large fibres (neurophysiology) or are invasive (skin/nerve biopsy). Unfortunately, diabetic neuropathy lacks a non-invasive surrogate for nerve damage. However, recent research [1, 2, 3] using corneal confocal microscopy (CCM) suggests that this non-invasive and hence reiterative test might be an ideal surrogate endpoint for human diabetic neuropathy. Studies in patients with diabetic neuropathy demonstrate that CCM accurately quantifies corneal nerve fibre morphology and reflects the severity of peripheral neuropathy. Corneal nerve damage results in loss of corneal sensitivity [4]. Assessment using CCM provides measures related to the severity of intra-epidermal nerve-fibre loss [5], and is capable of detecting early regeneration of small nerve fibre following, for example, pancreas transplant in diabetic patients [6]. The establishment of CCM as a surrogate for early diagnosis as an early biomarker for diabetic neuropathy could identify those at risk and prompt more intense intervention with standards of care including improved glycaemic, blood pressure and lipid control. Furthermore a sensitive surrogate endpoint would significantly lower hurdles to the development of disease-modifying therapeutics by enhancing the capacity to test therapeutic efficacy. The major advance of CCM is the entirely non-invasive and rapid (2 minutes) acquisition of images of small nerve fibres in patients. However, the major limitation preventing extension of this technique to wider clinical practice is that analysis of the images using interactive image analysis is highly labour-intensive ($\simeq 1.5$hrs) and requires considerable expertise to quantify nerve pathology. To be clinically useful as a diagnostic tool, it is essential that the measurements be extracted automatically.

Clearly an important stage in CCM images (an example is shown in 1(a)) is the detection of linear structures. A heuristic approach [7], using a method previously applied to detecting blood-vessels in retinal images, has been used for detecting fibres in CCM images. If CCM image analysis is to be applied clinically, especially to define early degeneration or regeneration, then a key step is the detection of low-contrast fibres among image noise. A method of linear structure detection (*linear operator* - Linop), originally developed for detection of asbestos fibres [8] has more recently been shown to effective in detecting ducts in mammograms [9]. Linop exploits the linear nature of the structures to enhance their contrast. Figure 1(c), shows the method applied to a CCM image containing low-contrast fibres. Among the many applications of Gabor wavelets has been the enhancement of the ridge-valley structure in fingerprint images [10]. This application has some commonality with the fibre-detection problem. In this paper we introduce the Gabor-wavelet enhancement for fibre detection in CCM images (Figure 1(d)) and present a comparative evaluation of the method and Linop.

2 Nerve Fibre Structure Enhancement

Normally CCM images are presented in a noisy environment. This is due to a number of factors. First the movement of the eye while capturing the image causes a motion blurring effect. Second the illumination effect caused by the capturing process itself. And finally, is the spherical shape of the cornea causes a spatial deformation if the distance between the lenses and the surface of the eye changes. Given that the general shape of the nerve fibre is known, the Gabor filter can enhance the contrast of the image due to its spatial response resemblance of the nerve fibre shape. It is also a band-pass filter that can help reduce some of the artefacts mentioned above.

*Email: m.a.dabbah@manchester.ac.uk

2.1 Local Orientation Estimation

In CCM images, the nerve fibres flow in locally constant orientations everywhere, called *local nerve orientation*. In addition, there is a global orientation that dominates the general flow. The orientation field describes the coarse structure of nerve fibres in the CCM images and has been proven to be of a fundamental importance in many image analysis applications [11,12] . Using the least mean square algorithm [10], the local orientation θ_{ij} of the block centred at pixel (i,j), Equation (3), is computed using the following equations [11],

$$\mathcal{V}_x(i,j) = \sum_{u=i-\frac{\omega}{2}}^{i+\frac{\omega}{2}} \sum_{v=j-\frac{\omega}{2}}^{j+\frac{\omega}{2}} \left(\partial_x^2(u,v) - \partial_y^2(u,v)\right) \tag{1}$$

$$\mathcal{V}_y(i,j) = \sum_{u=i-\frac{\omega}{2}}^{i+\frac{\omega}{2}} \sum_{v=j-\frac{\omega}{2}}^{j+\frac{\omega}{2}} 2\partial_x(u,v)\partial_y(u,v) \tag{2}$$

$$\theta_{ij} = \frac{\pi}{2} + \frac{1}{2}\tan^{-1}\left(\frac{\mathcal{V}_y(i,j)}{\mathcal{V}_x(i,j)}\right) \tag{3}$$

The gradients $\partial_x(u,v)$ and $\partial_y(u,v)$ are computed at each pixel (u,v) and may vary from the simple *Sobel* operator to the more complex *Canny* operator depending on the computational requirements. ω is the width of the block centred at pixel (i,j). The orientation field is then smoothed by convolving the x and y vector field components in Equation (4) and Equation (5) respectively, with a low-pass Gaussian filter. This smoothed orientation field is calculated by Equation (8), where $\hat{\Phi}_x(i,j)$ and $\hat{\Phi}_y(i,j)$ are the smoothed continuous x and y vector field components.

$$\Phi_x(i,j) = \cos\left(2\theta_{ij}\right) \tag{4}$$

$$\Phi_y(i,j) = \sin\left(2\theta_{ij}\right) \tag{5}$$

According to the original algorithm [10], the low-pass 2-dimensional Gaussian filter $\mathcal{G}$ is applied on the block level ω of the orientation field computed earlier in Equation (3). The filter has a unit integral and a kernel size of $\omega_\Phi \times \omega_\Phi$. However, since the orientation in CCM images varies at a slower rate than in fingerprint images, the low-pass filter is applied globally in order to further reduce errors at near-nerve fibre and non-nerve fibre regions. This operation is done due to the presence of noise, corrupted nerve structures and optical deformation. The estimated orientation is not always correct hence the low-pass filter tries to rectify the error given that the orientation in the local neighbourhood varies slowly;

$$\hat{\Phi}_x(i,j) = \sum_{u=-\frac{\omega_\Phi}{2}}^{\frac{\omega_\Phi}{2}} \sum_{v=-\frac{\omega_\Phi}{2}}^{\frac{\omega_\Phi}{2}} \mathcal{G}(u,v)\Phi_x(i-u,j-v) \tag{6}$$

$$\hat{\Phi}_y(i,j) = \sum_{u=-\frac{\omega_\Phi}{2}}^{\frac{\omega_\Phi}{2}} \sum_{v=-\frac{\omega_\Phi}{2}}^{\frac{\omega_\Phi}{2}} \mathcal{G}(u,v)\Phi_y(i-u,j-v) \tag{7}$$

$$\mathcal{O}_{ij} = \frac{1}{2}\tan^{-1}\left(\frac{\hat{\Phi}_y(i,j)}{\hat{\Phi}_x(i,j)}\right) \tag{8}$$

The least square estimate produces a stable smooth orientation field in the region of the nerve fibres. However, when applied on the background of the image i.e. between fibres, the estimate is dominated by noise due to the lack of structure and uniform direction, which is expected and understandable. Figure 1(a) and Figure 1(b) show the original CCM image and its orientation field estimate using the least square method respectively.

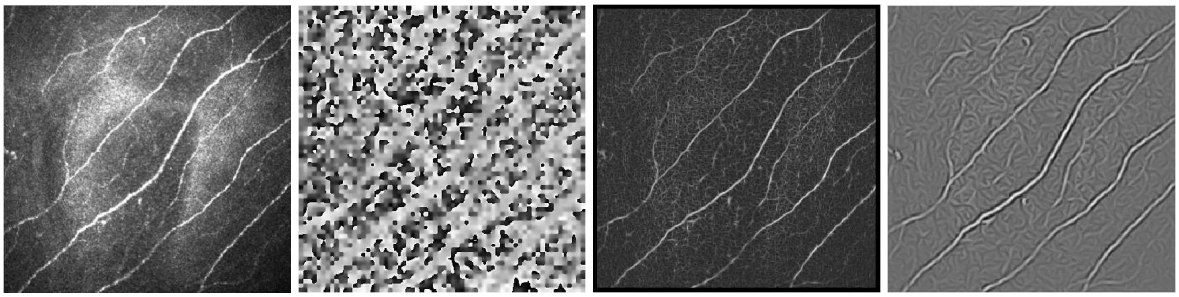

(a) Original image (b) Orientation field (c) Linop response (d) Gabor response

Figure 1. An illustration of the least square estimate orientation (b) and the responses of the Linop algorithm (c) and the Gabor filter (d) for the CCM image in (a).

2.2 Spatial Domain Enhancement

Spatial domain enhancement is based on the convolution of the image with the even-symmetric Gabor filter [13] that is tuned to the local nerve fibre orientation Figure 2. The Gabor filter is a two-dimensional band-pass filter that consists of a sinusoidal plane wave with certain orientation and frequency, modulated by a Gaussian envelope.

$$h(x, y, \phi, f) = \exp\left\{-\frac{1}{2}\left[\frac{x_\phi^2}{\sigma_x^2} + \frac{y_\phi^2}{\sigma_y^2}\right]\right\}\cos(2\pi f x) \tag{9}$$

$$x_\phi = x\cos\phi + y\sin\phi \tag{10}$$

$$y_\phi = -x\sin\phi + y\cos\phi \tag{11}$$

where ϕ is the orientation of the Gabor filter, f is the frequency of the cosine wave, σ_x and σ_y are the standard deviations of the Gaussian envelope along the x and y axis, respectively. x_ϕ and y_ϕ define the x and y axis of the filter coordinate frame after a clockwise rotation of the Cartesian axis by the an angle of $\left(\frac{\pi}{2} - \phi\right)$. The Gabor filter enhances

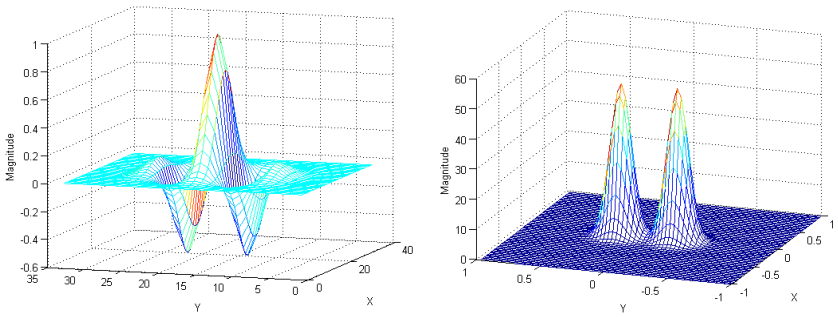

(a) Spatial domain (b) Frequency domain

Figure 2. The impulse response of the spatial two-dimensional Gabor kernel is shown in (a) while its FFT response is shown in (b).

the nerve fibres that are oriented in its direction, and decreases anything that is oriented differently. This increases the contrast between the foreground and the noisy background, whilst effectively reducing noise around the fibre structure. Another advantage of this operation is increasing the possibility of detecting nerve fibres with very little contrast. This is due to the prior knowledge of the general structure of the fibre and the assumption of the continuous flow of the fibres along a particular known direction.

3 Experimental Results

The experiments were conducted on 12 CCM images that were captured using the HRT-III [1] microscope. Six of the images are control subjects and the rest from patients with different neuropathic severity. The images have a size of

[1]The Heidelberg Retina Tomograph confocal scanning laser ophthalmoscope developed by Heidelberg Engineering Inc. The instrument can be converted into a confocal corneal microscope using a microscope lens which is attached to the standard lens.

384×384 pixels, 8-bit grey levels and stored in BMP format. The resolution is $1.0417\mu m$ and the field of view is $400 \times 400\mu m^2$ of the cornea. The performance of both methods is obtained by validating the extracted nerve fibres using ground truth data that has been manually generated. Only the raw response of each method is taken into account without any further post-processing operations or shade correction methods, Figure 1(c) and Figure 1(d). Binary images are obtained by a simple uniform thresholding operation and followed by a thinning operation [14] to achieve a one-pixel-wide skeleton image. Both methods have been allowed a tolerance of $\pm 3.141\mu m$ in nerve fibre location precision. Three measures have been used in order to quantify the evaluation. The false positive (FPR), the false negative (FNR) and the equal error rate (EER), which is the average of optimal FPR and FNR at minimal difference between both. The measurements are taken by comparing the generated skeleton at different threshold intervals of the methods' responses. Table 1 presents the average error rates and shows that the mean EER for the Gabor filter is reduced by 11.82% over

	Linop				Gabor			
	μ_l	σ_l^2	$\mathbf{max}_l$	$\mathbf{min}_l$	μ_g	σ_g^2	$\mathbf{max}_g$	$\mathbf{min}_g$
False Positive$_{[\%]}$	25.22	59.16	34.04	13.24	21.90	43.33	30.38	12.95
False Negative$_{[\%]}$	25.03	58.15	33.74	12.66	22.41	49.89	31.71	13.15
Equal Error$_{[\%]}$	25.12	58.52	33.89	12.95	22.15	46.46	30.84	13.05

Table 1. The error rates of the Linop and the Gabor algorithms.

Linop. The variance of the error rates was also reduced by 20.06% ,which indicates a more stable behaviour for the Gabor method. However, Linop has obtained the lowest error rate of a single image. As shown, both methods have high error rates due to the nature of the CCM images and the faint nerve fibre structure, which increases the FNR and in turn demands more sensitive filtering response that increases the FPR. The behaviour of the FPR and the FNR curves

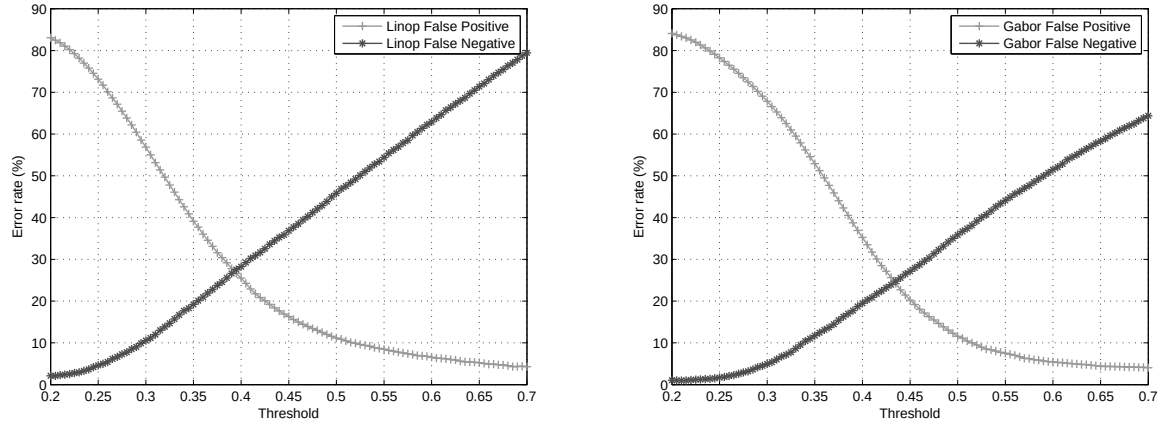

(a) Linop performance (b) Gabor performance

Figure 3. The false positive and false negative curves of Linop (a) and Gabor (b).

with respect to the selected threshold is shown in Figure 3. The optimal threshold for Linop is $\simeq 0.395$ and for Gabor is $\simeq 0.435$. Generally, the curves of the Gabor method maintain a lower rate than Linop's curves. As shown by the ROC curves (Figure 4), the Gabor method has outperformed the Linop method with slight overall improvement. This is mainly due to the response of the Gabor filter and its adaptive orientation at each pixel. This adaptive feature forces the filter to enhance the region of the image according to the general direction computed by the least square algorithm, which does not significantly vary in local neighbourhoods, whereas Linop takes the maximum response of the region and registers the direction of this response as the orientation of the neighbourhood. In the case of low-contrast lines, this maximum response could be due to noise.

4 Conclusion

As the significance of understanding the CCM in detecting and quantifying both diabetic and other neuropathics increases, an automated image analysis system becomes more desirable in order to ensure accuracy, reliability, consistency and convenience to both patients and clinicians. This paper has presented a comparison between two methods for nerve fibre detection. The Gabor method has outperformed the Linop method with a 11.82% reduction in the EER. Although the EER is still too high for accurate detection, the performance can be boosted by a post-processing operation, which immediately enhances the FPR and allows tuning of the detection procedure in order to avoid false negatives.

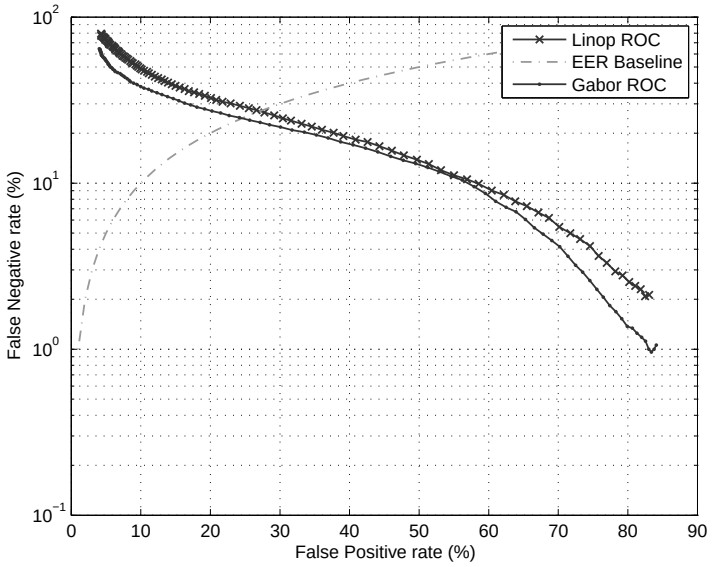

Figure 4. The receiver operating characteristic (ROC) curves of Linop and Gabor.

Acknowledgements

This work is supported by a JDRF scholar grant 17-2008-1031.

References

1. R. A. Malik, P. Kallinikos, C. A. Abbott et al. "Corneal confocal microscopy: a non-invasive surrogate of nerve fibre damage and repair in diabetic patients." *Diabetologia* **46(5)**, pp. 683–688, 2003.
2. P. Kallinikos, M. Berbanu, C. O'Donnell et al. "Corneal nerve tortuosity in diabetic patients with neuropathy." *Investigative Ophthalmology & Visual Science* **45(2)**, pp. 418–422, Feb. 2004.
3. P. Hossain, A. Sachdev & R. A. Malik. "Early detection of diabetic peripheral neuropathy with corneal confocal microscopy." *The Lancet* **366(9494)**, pp. 1340–1343, 2005.
4. M. Tavakoli, P. A. Kallinikos, N. Efron et al. "Corneal sensitivity is reduced and relates to the severity of neuropathy in patients with diabetes." *Diabetes Care* **30(7)**, pp. 1895–1897, Jul. 2007.
5. C. Quattrini, M. Tavakoli, M. Jeziorska et al. "Surrogate markers of small fiber damage in human diabetic neuropathy." *Diabetes* **56(8)**, pp. 2148–2154, Aug. 2007.
6. S. Mehra, M. Tavakoli, P. A. Kallinikos et al. "Corneal confocal microscopy detects early nerve regeneration after pancreas transplantation in patients with type 1 diabetes." *Diabetes Care* **30(10)**, pp. 2608–2612, Oct. 2007.
7. A. Ruggeri, F. Scarpa & E. Grisan. "Analysis of corneal images for the recognition of nerve structures." pp. 4739–4742. Sep. 2006.
8. R. N. Dixon & C. J. Taylor. "Automated asbestos fibre counting." In *Machine Aided Image Analysis*, pp. 178–185. Institute of Physics, London, 1979.
9. R. Zwiggelaar, S. Astley, C. Boggis et al. "Linear structures in mammographic images: Detection and classification." *IEEE Transactions on Medical Imaging* **23(9)**, pp. 1077–1086, Sep. 2004.
10. L. Hong, Y. Wan & A. Jain. "Fingerprint image enhancement: algorithm and performance evaluation." *IEEE Transactions on Pattern Analysis and Machine Intelligence* **20(8)**, pp. 777–789, Aug 1998.
11. A. R. Rao. *A taxonomy for texture description and identification*. Springer-Verlag New York, Inc., New York, USA, 1990.
12. M. Kass & A. Witkin. "Analyzing oriented patterns." *Computer Vision, Graphics & Image Processing* **37(3)**, pp. 362–385, 1987.
13. A. K. Jain & F. Farrokhnia. "Unsupervised texture segmentation using gabor filters." *Pattern Recognition* **24(12)**, pp. 1167–1186, 1991.
14. L. Lam, S.-W. Lee & C. Suen. "Thinning methodologies-a comprehensive survey." *IEEE Transactions on Pattern Analysis and Machine Intelligence* **14(9)**, pp. 869–885, Sep. 1992.